Relating Atomistic Grain Boundary Simulation Results to the Phase-Field Model

Catherine M. Bishop * W. Craig Carter

Department of Materials Science and Engineering,

Massachusetts Institute of Technology,

77 Massachusetts Ave., Cambridge, MA 02139

Abstract

A coarse-graining method for mapping discrete data to a continuous structural order parameter is presented. This method is intended to provide a useful and consistent method of utilizing structural data from molecular simulations in continuum models, such as the phase field model. The method is based on a local averaging of the variation of a Voronoi tessellation of the atomic positions from the Voronoi tessellation of a perfect crystal (the Wigner-Seitz cell). The coarse-graining method is invariant to coordinate frame rotation. The method is illustrated with a simple two-dimensional example and then applied to a three-dimensional relaxation simulation using the silicon EDIP potential of a $\Sigma 5$ grain boundary. Calculated results indicate that a continuous structural parameter is obtained that has grain boundary characteristics similar to phase field models of grain boundaries. Comparisons to other coarse-graining measures of structure are discussed as well as applications

to experimental data sets.

Key words: coarse-graining, phase-field model, Voronoi tessellation, grain boundary

PACS: 61.43.B, 07.05.T, 68.35

---

1 Introduction

In this paper we describe an algorithm for coarse-graining to generate structural order parameters. Coarse-graining is the first step in deriving a continuum model, such as the phase-field model from microscopic physics or atomistic data. Furthermore, the method is reference-frame invariant which is important as we discuss below.

The phase-field model has been used to study dendritic solidification of binary alloys, phase changes in ternary systems, grain growth in single component solids, equilibrium shapes of a particle in a matrix, and grain growth with anisotropic mobilities and grain boundary energies [1–6].

The basic premise of the phase-field model is that the phase fields represent some coarse-graining of a physical system, or averaged physical system, composed of an ensemble of atoms. The parameter fields are considered to vary continuously as a function of position whether the system is in equilibrium or

* Corresponding author: Phone 617.258.5551 Fax 617.258.7874
Email address: cbishop@mit.edu (Catherine M. Bishop).

not. Continuity of parameters results in a "diffuse interface" that represents the average spatial variation of a field but is understood to represent a set of atomic coordinates. Typically, these atoms are represented by discrete points in space. For example, physical measurements of composition or of the structure of a system are an averaging of this atomic data in space and also in time. Molecular Dynamics (MD) or Monte Carlo (MC) experiments are a time or phase space average, respectively, of discrete data such as atomic positions. In order to compare atomistic simulation data to the phase-field model some averaging must take place.

A phase-field model derives from a free energy functional that depends on the phase fields, $\phi_i(\vec{x})$, and ought to be constructed so that it is consistent with observed phenomena and underlying physical behavior. The total energy, Eq. 1, is written as an integral of the homogeneous energy density, $f(\phi_i(\vec{x}))$, and gradient energy terms that intrinsically account for interfacial energies. The interface is "smoothed" with typically square gradient energy penalties.

$$F = \int_\Omega \left[f(\phi_i(\vec{x})) + \sum_i \kappa_i |\nabla \phi_i|^2 \right] dV \tag{1}$$

The evolution of the system assures a monotonic decrease in Eq. 1 and is determined by the evolution of the set of fields that describe it. Level sets of ϕ_i can be used to track interfaces.

A phase-field is a continuous description of one property of a physical system. Multiple fields are used to study complex systems. For studies of grain

growth, Kobayashi, Warren and Carter (KWC) use a phase-field model with two fields: the degree of crystalline order, $\eta(\vec{x})$, and the crystallographic orientation, $\theta(\vec{x})$, that represents a rotation with respect to a particular laboratory frame [4]. It should be noted that here the homogeneous energy density is correctly reference-frame invariant. In this model, a grain boundary has a particular signature in the two fields, $\eta(\vec{x})$ and $\theta(\vec{x})$. Suppose a grain boundary is located at $x = 0$ and runs parallel to the y-axis, the orientation $\theta(x)$ then changes abruptly in the vicinity of $x = 0$ to values representative of the abutting grain orientations, while the crystallographic order exhibits a significantly less localized dip with a local minimum at the boundary position. MD simulations exhibit behavior that is qualitatively similar [7,8]. This paper describes a method that quantifies such comparisons.

Other models of grain growth that are not reference-frame invariant, such as those proposed by Venkitachalam *et al.* and Kazaryan *et al.* , have a finite set of long-range order parameters (LRO), $\eta_i(\vec{x})$, representing the distinct orientations for each grain [9,10]. Khachaturyan has suggested a method for extracting structural information, a LRO parameter, from atomistic coordinates [11]. However, this method is not reference-frame invariant and the multiple fields from such a method are neither necessary nor correct in resulting formulations of phase-field models for grain growth.

Khachaturyan's method defines a reference-frame dependent LRO parameter for each grain orientation in a simulation. For a system of grains with p dis-

tinct orientations, this results in a phase-field representation with p fields and evolution equations. This method also prohibits the grain rotation which has been observed experimentally, for example, in gold thin films, in 2-D nanocrystalline MD grain growth simulations, and is naturally included in the KWC method [12,13,4]. Grain rotation is expected in fine-grained materials.

The radial distribution function (RDF) is used to look for non-crystalline structures by examining the second-nearest neighbor peak. This method is reference-frame invariant but loses the angular information that is required in the KWC model in addition to generating a spatially averaged distribution rather than a position dependent order-parameter field.

Other reference-frame invariant methods of characterizing structure such as bond-center distributions, angle-cosine distributions, and invariants of spherical harmonics are reviewed by McGreevy [14]. The bond center distribution method assigns points to the center of the vectors connecting neighboring atoms and the structure factor or radial distribution function of these is then used to characterize the order. The angle-cosines of the vectors between neighboring atoms are calculated to generate bond angle distributions that give insight into the dominant local symmetry. Steinhardt *et al.* introduced spherical harmonics in the description of short-range order in liquid and glass structures [15]. Comparison of the Steinhardt's distribution in a sample to known distributions for reference samples gives an indication of local ordering. Van Duijneveldt and Frenkel use a rotationally invariant combination of spherical

harmonics averaged over all atoms, Q_6, as an orientational order parameter [16]. This single number is chosen as it is relatively insensitive to crystal structure but at the same time sensitive to local order and disorder. Steinhardt's method has been generalized with the use of Legendre polynomials by Rodriguez de la Fuente and Soler [17].

The methods described above generate either a distribution or a single order parameter to characterize the whole sample. The goal of this work is to find a method of turning discrete atomic data into a field parameter, $\eta(\vec{x})$ of the KWC phase-field model, that smoothly varies in space and measures short range order.

An alternate way of characterizing the structure of a material in a reference-frame independent scheme is to utilize a geometric method. Several authors have dismissed the use of Voronoi tessellations in the characterization of order in materials but have only considered the usefulness of the Voronoi histogram which is very sensitive to small perturbations of the atomic positions [16,18]. However, Voronoi tessellations have been used extensively for material characterization at the microstructural length-scale and to examine single and multiple component atomic structures [19–21]. An anisotropy factor, typically a non-sphericity, is calculated as a ratio of tessellation properties and used in a statistical analysis.

One such analysis of single-component ordered and disordered structures was

completed by Montoro and Abascal [20]. The authors performed 3-D simulations using a Lennard-Jones potential to produce data structures that they characterize as solid, liquid, quenched liquid, and gas. The Voronoi tessellation is calculated for each atom in a structure and the non-sphericity, α, given in Eq. 2, is calculated where V is the volume, S is the surface area, and R is the average radius of curvature of the convex body. The average radius of curvature for a polyhedron is given in Eq. 3 where the sum is over the edges, l_i is the length of the ith edge, and ϕ_i is the angle between the faces intersecting the ith edge. The authors distinguish the different structures by examining the histogram of the anisotropy factors.

$$\alpha = \frac{RS}{3V} \tag{2}$$

$$R = \frac{1}{8\pi} \sum_{i}^{\text{edges}} l_i \phi_i \tag{3}$$

For each crystal structure there is a characteristic value of the anisotropy factor for the Wigner-Seitz cell (Voronoi tessellation for the crystal). For example, for a simple cubic crystal structure, the Wigner-Seitz cell is a cube with $\alpha_{ws} = \frac{3}{2}$. For non-crystalline structures the anisotropy factor has a dispersion that characterizes a disordered system as shown in Fig. 1. Note that the average values of α for the quenched liquid, liquid, and gas structures are greater than α_{ws}.

In this paper we describe a method for reducing the wealth of data available at the small scale to data sets needed at the larger scale of the phase-field.

The small scale data sets are discrete while the phase-field description requires continuous and differentiable data. Particularly, we present a method of analyzing atomistic data to produce a reference-frame invariant measure of short-range structure, such as the $\eta(\vec{x})$ parameter in the KWC model, using Voronoi tessellations [4]. The method is first defined in general terms for a single component solid structure and is then applied to a relaxed $\Sigma 5$ grain boundary from a simulation at 0K in diamond cubic silicon. While the method is applied to a particular system, this paper aims to describe a general method of coarse-graining atomistic data. Our purpose is to find a meaningful way of extrapolating data.

2 Method

2.1 General

In this section we describe a general method for coarse-graining atomic structure information to a continuum SRO parameter. The results from an MD or MC simulation are a set of atomic positions, usually in three dimensions. To illustrate the method it is useful to describe its application to a two-dimensional MD grain boundary equilibration for a Lennard-Jones solid, although it is applied below to a three-dimensional data set.[1] From the list of positions, the

[1] The description of the algorithm is in three-dimensions, but the illustration in Fig. 2 is in two. The reduction is straightforward.

Voronoi tessellation for each atom is constructed using Qhull [22], a convex hull calculation code, and stored, as shown in Fig. 2. Qhull calculates the surface area and volume of each tessellation. Using output from Qhull, required geometric quantities, such as the mean curvature and anisotropy factor, were calculated for each tessellation.

A cubic mesh of a given size is laid over the data so that at least 100 mesh points fall within each tessellation. Each mesh point is assigned an anisotropy factor, α_{ijk} where ijk reference the mesh point, based on the tessellation in which it falls. Next, the center of a measurement volume or aperture is placed at some position in space, $\vec{x}$, where the averaging is to be assigned. The value of the anisotropy factor at this point, $\tilde{\alpha}(\vec{x})$, is the average over all the α_{ijk} that fall within the measurement aperture.

This averaged anisotropy factor, $\tilde{\alpha}(\vec{x})$, can be compared to that for the Wigner-Seitz cell, α_{ws}, to generate a coarse-grained measure of the crystalline SRO called $\eta(\vec{x})$. Disordered solid structures may have $\tilde{\alpha}(\vec{x}) > \alpha_{ws}$ or $\tilde{\alpha}(\vec{x}) < \alpha_{ws}$. The proposed scaling in Eq. 4, which has an upper bound of $\eta(\vec{x}) = 1$ but no lower bound, naturally handles either case, Fig. 3. For the case when $\tilde{\alpha}(\vec{x}) = \alpha_{ws}$ and $\eta(\vec{x}) \equiv 1$, this corresponds to the definition of the crystalline solid as described in the KWC model [4].

$$\eta(\vec{x}) \equiv 1 - \frac{|\alpha_{ws} - \tilde{\alpha}(\vec{x})|}{\alpha_{ws}} \tag{4}$$

The above method for coarse-graining is applied to the specific example of a $\Sigma 5$ grain boundary in diamond cubic silicon. The equilibrium configuration of a $\Sigma 5$ boundary at $T = 0$K and $P = 0$Pa was computed on a 3-D periodic simulation cell in silicon using the EDIP potential developed by Bazant *et al.* [23,24]. The results are qualitatively similar to previous numerical experiments, for example [8,25]. The orthorhombic cell with $\sigma_{zz} = 0$ containing two grain boundaries (at $z = 0$ and $z = Z/2$) has cell dimensions $X = 8.577$Å, $Y = 8.577$Å, and $Z = 33.517$Å, or a 2.875% elongation in the z-direction. The purpose of obtaining this structure was the procurement of a data set to illustrate the procedure of relating atomic positions to a continuous field variable. The details of the simulation are less important than the relation of the results to a continuous order parameter.

The equilibrium atomic positions were input to Qhull to calculate the Voronoi tessellation of each atom. The anisotropy factor for each tessellation, α_i, was then calculated. Next, cubic meshes with spacings 0.5Å and 0.25Å were created with $\mathcal{O}(10^2)$ and $\mathcal{O}(10^3)$ mesh points per tessellation, respectively. The α_{ijk} at each mesh point was assigned. The meshes and the corresponding α_{ijk} values were stored in a file for use in further calculations.

Both cubic and spherical apertures with characteristic sizes $r = 1$Å and $r = 2$Å were used for averaging. The local value of $\tilde{\alpha}(\vec{x})$ was calculated from the

average of the mesh values within the aperture volume and scaled to $\eta(\vec{x})$ using Eq. 4. Profiles were calculated at constant height, (x, y, z_0), and also for variable height, (x_0, y_0, z), for both meshes with measurements spaced by 0.25Å in every case. The results are presented in the next section.

3 Results

Grain boundary profiles of $\eta(x_0, y_0, z)$ are presented in Figs. 4 and 5. The profiles $\eta(0, 0, z)$ traverse the boundary through a grain boundary coincidence lattice site in the unrelaxed structure. The other profiles at $(2, 2, z)$ and $(3.5, 3.5, z)$ pass through arbitrary points in the grain boundary. It should be noted that no computational calculation generates a truly continuous variable but only a variable that can be sampled anywhere in a domain such as this $\eta(\vec{x})$.

It is apparent that the 0.25Å mesh approximates the intersection of the aperture with each tessellation better than the 0.5Å mesh. The 2Å aperture generates a smoother profile than the 1Å aperture. Also, the spherical aperture produces a smoother profile than the cubic aperture. The smoothest profiles are generated for the 0.25Å mesh with a spherical aperture of radius 2Å. The larger aperture and smaller mesh size mean that more points are averaged for each measurement. The spherical aperture has higher symmetry than the cubic aperture, thus reducing geometric noise in the averaging.

These profiles show that there is some non-crystallinity between the center of each simulated grain and the center of the grain boundary. Just to the side of the center of each grain there is a small deviation from unity. This is an effect of the exact method of the relaxation simulation. The large deviation from unity is the hallmark of the grain boundary itself.

These profiles resemble those diffuse interfaces found in the phase-field model representing grain boundaries. The smaller the mesh size and the smaller the sampling distance, the smoother the grain boundary profiles should become. However, convergence is hard to define for this coarse-graining technique. For the "smoothest" profile (i.e., 0.25Å mesh and 2Å spherical aperture) the deviation from perfect SRO is 4.8% at $(2, 2, z)$. In contrast, the maximum variation within the (x,y,8) plane section (i.e., in the crystalline region) is 0.09%.

4 Discussion

The coarse-graining method above generates a short-range structural order parameter. The local measure of SRO in the system, not LRO, should control the structural contribution to the total energy. In fact, this is the basic assumption in the phase-field model: that the energy density is local. The local energy density is represented as the Taylor expansion of the homogeneous energy about small gradients in the phase fields. So the energy that is written for an infinitesimal volume element should be in terms of SRO for the structural

part. In other words, when comparing the energies of two infinitesimal regions in a material both with the structure of perfect crystal but the first surrounded by perfect crystal and the second by liquid-like structures, the difference in energy should come from the gradient energy terms in the functional.

Other characterization methods are unsuitable for the generation of $\eta(\vec{x})$ in this application. The RDF contains no angular information and is a distribution not a scalar or vector field. Bond-center and bond-angle distribution functions are unsuitable as they also output a distribution. The methods based on spherical harmonics are non-local in the sense that they generate a single reaction coordinate to characterize the short-range orientational order, not a position dependent field. However, it may be possible to construct a method of generating an order-parameter field derived from the spherical harmonics but the method presented here is computationally and conceptually straightforward.

In this method, the mesh is used as a way of approximating the geometry of each tessellation. The best method is to find the exact intersection of the measuring aperture and each tessellation. This is straightforward for the cubic aperture using Qhull. However, in order to find the intersection with the spherical aperture, the sphere must be approximated as a convex polyhedron with very many faces. Finding the intersection of the volumes is equivalent to finding the convex hull of the tessellation and the approximated sphere. Qhull is capable of this but is much slower than the proposed stored-mesh method

and must be performed for every sampling.

Another possible averaging technique is to spread the properties of each atom out in space according to a Gaussian relation. In other words, treat the anisotropy factor like a position dependent quantity with a probability density given by a Gaussian distribution. The averaged anisotropy factor at a point $\vec{x}$ is given by:

$$\tilde{\alpha}(\vec{x}) = \sum_i \frac{\alpha_i}{\sigma\sqrt{2}\pi} \exp\left[\frac{-(\vec{x} - \vec{x}_i)^2}{2\sigma^2}\right] \tag{5}$$

In the above, the sum is over all the atoms i, α_i is the anisotropy factor of the tessellation corresponding to the atom, $\vec{x}_i$ is the location of the atom, and σ is the standard deviation of the distribution or a measure of the spread. We attempted to use this method but $\tilde{\alpha}(\vec{x})$ doesn't exhibit the required uniform value in a perfect crystal, even for large σ.

The coarse-graining method demonstrated in this paper has been illustrated for a single component solid simulation. The same method is equally applicable to multicomponent substitutional solid solutions as long as the atomic radii of species are similar. Then the geometry of the Voronoi tessellation of every atom in the perfect crystal at any composition is identical. The composition is measured with another phase-field and so should not be taken into account in the structural measure.

The scaling from $\tilde{\alpha}(\vec{x})$ to $\eta(\vec{x})$ here, Eq. 4, is sufficient for solid systems with some structural disorder. However, it is possible that liquids and gases will

have $\alpha(\vec{x}) > 2\alpha_{ws}$ and, therefore, $\eta(\vec{x}) < 0$, Fig. 1. For liquids and gases, a normalizing value different from α_{ws} may be needed, such as the average $\alpha(\vec{x})$ for the liquid or gas.

The coarse-graining method was illustrated with an example of a simulated grain boundary relaxed at zero temperature. For non-zero temperature simulations, there is a further complication due to thermal noise.

In MC simulations, phase space is sampled using, for example, the Metropolis algorithm to hone the sampling. After a large number of steps, the equilibrium state is that which has the most occurrences in phase space. This equilibrium configuration, set of positions, can be input directly into the coarse-graining method.

However, for MD, the atoms are moved around according to the force on each atom. When the total energy converges to a roughly constant (minimum) value or the force on each atom drops below some limit, the system is taken to be equilibrated for constant temperature simulations. However, thermal vibrations (Debye-Waller effect) mean that the atoms are moving about their equilibrium positions. Commonly, the trajectories of the atoms are then followed and averaged to give the equilibrium positions which may be input to the coarse-graining method.

One problem with the phase-field model is the artificial spreading of the interface. Using this coarse-graining method, the structural width of the interface

is also increased. This method, therefore, allows a direct comparison between atomistic grain boundary simulations and phase-field simulations. Boundary energies, widths, and mobilities can be computed from a phase-field model and matched to those generated from coarse-graining simple atomistic simulations. This will allow for the incorporation of small-scale physics into larger-scale phase-field calculations on complicated microstructures.

The relatively new three-dimensional atom probe (3DAP) provides data on the spatial distribution of chemical species evaporated from the tip of a probe [26,27]. The spatial resolution of the technique is 2Å laterally and 0.6Å in the perpendicular direction for a pure metal [26]. The effectiveness of this method applied to ceramic systems exhibiting intergranular glassy films should be limited by thermal effects and the difference in ionization potentials for the constituents. However, using MD or MC experiments in concert with 3DAP can provide data sets for coarse-graining. These results can be used to develop phase-field models.

5 Conclusions

A structural method for coarse-graining discrete atomic data to produce a continuous, differentiable measure of SRO using Voronoi tessellations has been developed. The method was applied to simulation results for a $\Sigma 5$ grain boundary in silicon. The coarse-grained profiles of the structural order parameter,

$\eta(x_0, y_0, z)$, reveal a smooth profile across the interface similar to the results of phase-field simulations [4].

The method as described above can be applied readily to MD or MC simulations of any multicomponent, iso-structural, solid system. The normalization may need to be adjusted for application to liquid and gas systems. The method is reference-frame invariant as it is based on the geometric properties of the Voronoi tessellations of discrete atomic positions and produces a continuous parameter suitable for phase-field simulation.

6 Acknowledgments

This work was supported by National Science Foundation Grant NMR 0010062 and the Singapore-MIT Alliance. The authors gratefully acknowledge helpful discussions with Rowland Cannon and R. Edwin García.

References

[1] J. A. Warren and W. J. Boettinger, "Prediction of dendritic growth and microsegregation patterns in binary alloy using phase-field method," *Acta Metallurgica and Materialia*, vol. 43, pp. 689–703, 1995.

[2] D. J. Eyre, "Cascades of spinodal decomposition in the ternary Cahn-Hilliard equations," in *Mathematics of Microstructure Evolution*, pp. 367–378, The

Minerals, Metals and Materials Society, 1996.

[3] J. W. Cahn and D. J. Eyre. Unpublished research.

[4] R. Kobayashi, J. A. Warren, and W. C. Carter, "A continuum model of grain boundaries," *Physica D*, vol. 140, pp. 141–150, 2000.

[5] J. J. Eggleston, G. B. McFadden, and P. W. Voorhees, "A phase-field model for highly anistotropic interfacial energy," *Physica D*, vol. 150, pp. 91–103, 2001.

[6] A. Kazaryan, Y. Wang, S. A. Dregia, and B. R. Patton, "Grain growth in systems with anisotropic boundary mobility: Analytical model and computer simulation," *Physical Review B*, vol. 63, p. 184102, 2001.

[7] D. A. Litton and S. H. Garofalini, "Molecular dynamics simulations of calcium aluminosilicate intergranular films on (0001) Al_2O_3 facets," *Journal American Ceramic Society*, vol. 83, pp. 2273–2281, 2000.

[8] P. Keblinski, D. Wolf, S. Phillpot, and H. Gleiter, "Role of bonding and coordination in the atomic structure and energy of diamond and silicon grain boundaries," *Journal of Materials Research*, vol. 13, pp. 2077–2098, 1998.

[9] M. K. Venkitachalam, L.-Q. Chen, A. G. Khachaturyan, and G. L. Messing, "A multiple-component order parameter phase field model for anisotropic grain growth," *Materials Science and Engineering A*, vol. 238, pp. 94–100, 1997.

[10] A. Kazaryan, Y. Wang, S. A. Dregia, and B. R. Patton, "Generalized phase-field model for computer simulation of grain growth in anistotropic systems," *Physical Review B*, vol. 61, pp. 14275–14278, 2000.

[11] A. B. Khachaturyan, "Long-range order parameter in field model of solidification," *Philosophical Magazine A*, vol. 74, pp. 3–14, 1996.

[12] K. E. Harris, V. V. Singh, and A. H. King, "Grain rotation in thin films of gold," *Acta Materialia*, vol. 48, pp. 2623–2633, 1998.

[13] A. J. Haslam, S. R. Phillpot, D. Wolf, D. Moldovan, and H. Gleiter, "Mechanisms of grain growth in nanocrystalline fcc metals by molecular-dynamics simulation." to be published in *Materials Science and Engineering A*, 2001.

[14] R. L. McGreevy, "Understanding liquid structures," *Journal of Physics: Condensed Matter*, vol. 3, pp. F9–F22, 1991.

[15] P. J. Steinhardt, D. R. Nelson, and M. Ronchetti, "Bond-orientational order in liquids and glasses," *Physical Review B*, vol. 28, pp. 784–805, 1983.

[16] J. S. van Duijneveldt and D. Frenkel, "Computer simulation study of free energy barriers in crystal nucleation," *J. Chem. Phys.*, vol. 96, pp. 4655–4668, 1992.

[17] O. Rodriguez de la Fuente and J. M. Soler, "Structure and stabilitiy of an amorophous metal," *Physical Review Letters*, vol. 81, pp. 3159–3162, 1998.

[18] P. Rein ten Wolde, M. J. Ruiz-Montero, and D. Frenkel, "Numerical calculation of the rate of crystal nucleation in a lennard-jones system at moderate undercooling," *J. Chem. Phys.*, vol. 104, pp. 9932–9947, 1996.

[19] S. Ghosh, Z. Nowak, and K. Lee, "Quantitative characterization and modelling of composite microstructure by Voronoi cells," *Acta Materialia*, vol. 45, pp. 2215–2234, 1997.

[20] J. C. G. Montoro and J. L. F. Abascal, "The Voronoi polyhedra as tools for structure determination in simple disordered systems," *J. Phys. Chem.*, vol. 97, pp. 4211–4215, 1993.

[21] B. J. Gellatly and J. L. Finney, "Characterisation of models of multicomponent amorphous metals: The radical alternative to the Voronoi polyhedron," *Journal of Non-Crystalline Solids*, vol. 50, pp. 313–329, 1982.

[22] C. B. Barber, D. P. Dobkin, and H. T. Huhdanpaa, "The quickhull algorithm for convex hulls," *ACM Trans. on Mathematical Software*, vol. 22, no. 4, pp. 469–483, 1996.

[23] M. Z. Bazant, E. Kaxiras, and J. F. Justo, "Environment dependent interatomic potential for bulk silicon," *Phys. Rev. B*, vol. 56, pp. 8542–8559, 1997.

[24] J. F. Justo, M. Z. Bazant, E. Kaxiras, V. V. Bulatov, and S. Yip, "Interatomic potential for silicon defects and disordered phases," *Phys. Rev. B*, vol. 58, pp. 2539–2554, 1998.

[25] M. Kohyama and R. Yamamoto, "Tight-binding study of grain boundaries in Si:Energies and atomic structures of twist grain boundaries," *Phys. Rev. B*, vol. 49, pp. 17102–17117, 1994.

[26] F. Vurpillot, G. D. Costa, A. Menand, and D. N. Seidman, "Structural analysis in three-dimensional atom probe: a fourier transform approach," *Journal of Microscopy*, vol. 203, pp. 295–302, 2001.

[27] O. C. Hellman, J. Füsing, J. T. Sebastian, and D. N. Seidman, "Atom-by-atom chemistry of internal interfaces: simulations and experiments," *Materials*

Science and Engineering C, vol. 15, pp. 13–15, 2001.

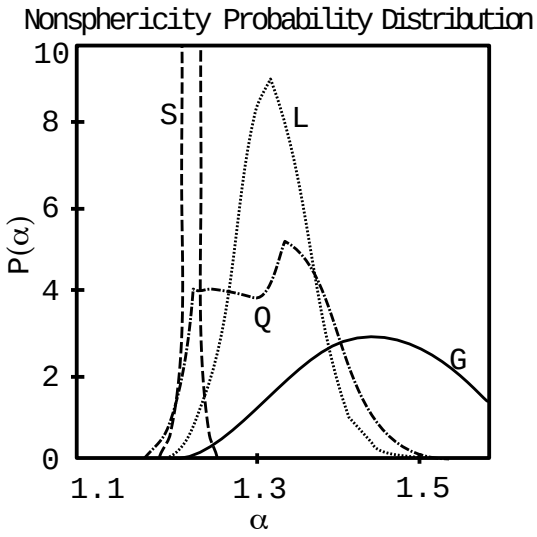

Fig. 1. Schematic of Fig. 6 from Montoro and Abascal showing non-sphericity for some generated structures [20]. S is solid curve, L liquid, G glass, and Q quenched liquid structure. The average α for each structure (except solid) is significantly larger than $\alpha_{ws} = 1.117$.

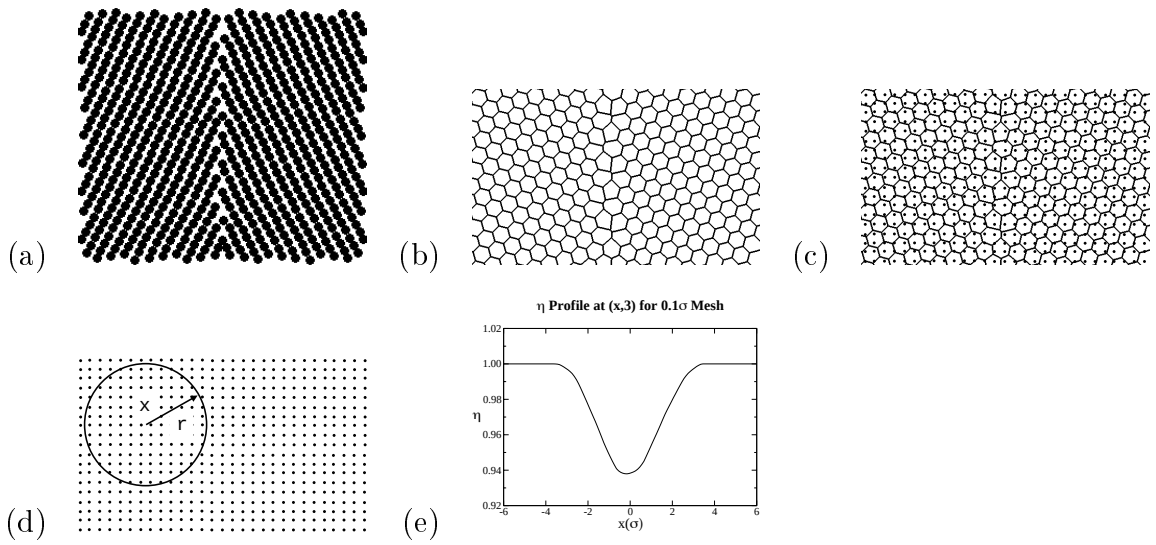

Fig. 2. Illustration of averaging method on averaged results of MD tilt boundary equilibration of Lennard-Jones solid. The anisotropy factor here is defined as $\beta = \frac{L^2}{A}$ where L is boundary length and A is area of the tessellation. We select this form instead of the two-dimensional equivalent of the non-sphericity, the non-circularity, because the mean radius of curvature for the Wigner-Seitz cell is identically zero. The normalization from $\beta(\vec{x})$ to $\eta(\vec{x})$ is chosen as $\eta = 1 - \frac{|\beta_{ws} - \beta(\vec{x})|}{\beta_{ws}}$. (a) Schematic of equilibrium-averaged atomic positions for complete set. (b) Voronoi tessellations are constructed from a central subset of positions. The anisotropy, β_i, is calculated for each tessellation. (c) A square mesh is laid over the tessellations. The value of β_{ij} for each mesh point is determined from the tessellation in which it lies. (d) The measurement aperture of size r is centered at (x, y) and the local value of $\tilde{\beta}(x, y)$ is the average of all mesh points that fall within the aperture. (e) Example of $\eta(\vec{x})$ profile perpendicular to grain boundary. Note local deviation of $\eta(\vec{x})$ in vicinity of grain boundary at $x = 0$.

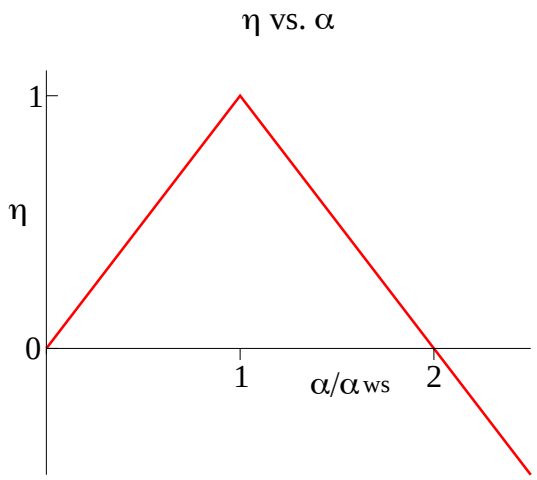

Fig. 3. Proposed scaling of $\alpha(\vec{x})$ to $\eta(\vec{x})$. Note that $\alpha(\vec{x}) > 0$ ($\eta(\vec{x}) < 1$) but there is no upper bound on $\alpha(\vec{x})$, or equivalently, no lower bound on $\eta(\vec{x})$.

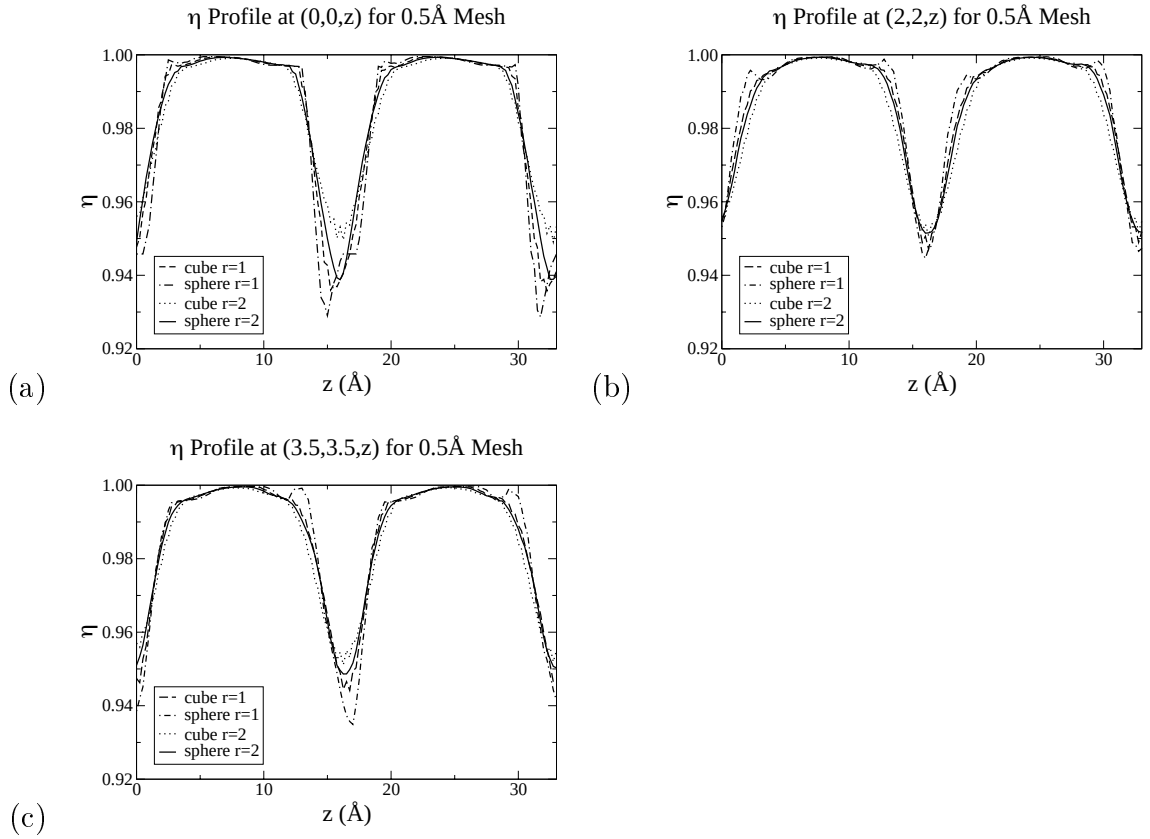

Fig. 4. Comparison of $\eta(\vec{x})$ profiles across the grain boundaries based on 0.5Å tessellation mesh with different aperture shapes and sizes. (a) at (0,0,z) (b) at (2,2,z) (c) (3.5,3.5,z).

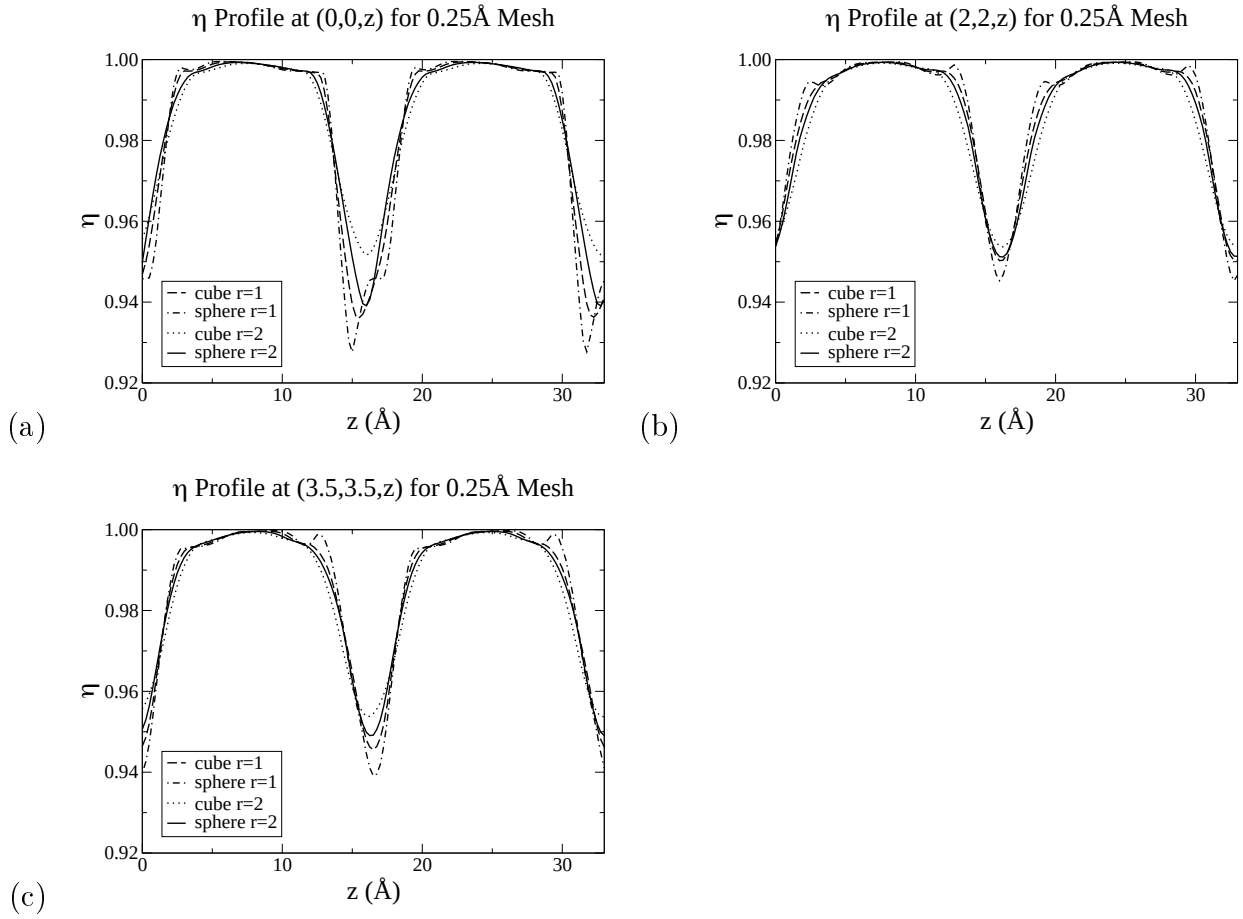

Fig. 5. Comparison of $\eta(\vec{x})$ profiles across the grain boundaries based on 0.25Å tessellation mesh with different aperture shapes and sizes. (a) at (0,0,z) (b) at (2,2,z) (c) (3.5,3.5,z).